Quantum Inf Process (2015) 14:3639–3659
DOI 10.1007/s11128-015-1080-3

A cellular automaton implementation of a quantum battle of the sexes game with imperfect information

Ramón Alonso-Sanz[1]

Received: 2 February 2015 / Accepted: 18 July 2015 / Published online: 4 August 2015

Abstract The dynamics of a spatial quantum formulation of the iterated battle of the sexes game with imperfect information is studied in this work. The game is played with variable entangling in a cellular automata manner, i.e. with local and synchronous interaction. The effect of spatial structure is assessed in fair and unfair scenarios.

Keywords Quantum games · Bayesian games · Entangling · Cellular automata

1 Introduction

Quantum game theory studies game theory with access to quantum technology [16,22,23,34]. It arose at the very end of the past century [14,26], ensuing since then a notable development. Controversy over what exactly a quantum game really is [8,9,17,19,20,33] and if there is indeed anything new for game theory [11,24] has been also present. This issue is not addressed here. Instead of it, we adopt in this article one of the most celebrated quantum game implementations, the EWL protocol introduced in [14]. The EWL method entangles strategies *à la* quantum, framing the study in the so-called *correlated games* [30,31], but allowing the players to actuate independently, as explained in Sect. 2.2.

This article deals with one of the most important asymmetric games: the battle of the sexes (BOS), described in Sect. 2, with players unsecure about the true desire of the opponent, i.e. with incomplete information, as explained in Sect. 3. In this study, the players are distributed in a two-dimensional lattice interacting in a simple form, i.e. in the cellular automaton (CA) manner introduced in Sect. 4. Quantum games

✉ Ramón Alonso-Sanz
ramon.alonso@upm.es

[1] Technical University of Madrid, ETSIA (Estadística, GSC). C. Universitaria, 28040 Madrid, Spain

have been recently studied operating in networks, but the study of quantum games embedded on spatial lattices, so with local interaction among players, is fairly absent (we have traced the Ref. [27]). The dynamics of such a spatialized BOS with imperfect information is analysed in the subsequent sections, paying particular attention to the effect that the variation of the degree of entanglement in the player strategies induces in the game dynamics.

The reader familiar with the CA literature should not confuse the quantum game CA approach proposed here (updated in a deterministic way) with general quantum CA models [37]. Besides, a disclaimer addressed to the quantum theory expert should emphasize that here we consider quantized games, but not the possibility of applying game theory to quantum mechanics, or gaming the quantum as proposed in [21].

2 The battle of the sexes with perfect information

The so-called *battle of the sexes* (BOS) is a simple example of a two-person (♀ and ♂) asymmetric game, i.e. a game whose payoff matrices are not coincident after transposition. Thus, for example: $\boldsymbol{P}_{♂} = \begin{pmatrix} R & 0 \\ 0 & r \end{pmatrix}$, and $\boldsymbol{P}_{♀} = \begin{pmatrix} r & 0 \\ 0 & R \end{pmatrix}$. The rewards $R > r > 0$ quantify the preferences in a conventional couple fitting the traditional stereotypes: the male prefers to attend a *F*ootball match, whereas the female prefers to attend a *B*allet performance. Both players decide hoping to *coordinate* their choices, but with *conflicting* interests, as $R \neq r$ [31,32].

2.1 The classic context

Using uncorrelated probabilistic strategies $\boldsymbol{x} = (x, 1-x)'$ and $\boldsymbol{y} = (y, 1-y)'$, the expected payoffs ($p$) in the BOS game are:

$$p_{♂}(x; y) = \boldsymbol{x}' \boldsymbol{P}_{♂} \boldsymbol{y}, \qquad p_{♀}(y; x) = \boldsymbol{x}' \boldsymbol{P}_{♀} \boldsymbol{y}. \tag{1}$$

The pair of strategies $(\boldsymbol{x}, \boldsymbol{y})$ are in Nash equilibrium (NE) if $\boldsymbol{x}$ is a best response to $\boldsymbol{y}$ and $\boldsymbol{y}$ is a best response to $\boldsymbol{x}$. The three NE in the BOS are achieved with: $x = y = 0$, $x = y = 1$, and $\big(x = R/R + r, y = 1 - x\big)$. If $y = 1 - x$, it is $p_{♂} = p_{♀}$, with maximum $p^+ = (R + r)/4$ for $x = y = 1/2$.

In a different game scenario, usually referred to as correlated games, the players have not an active role, instead of it an *external* a probability distribution $\boldsymbol{\Pi}$ assigns probability to every combination of player choices, so $\boldsymbol{\Pi} = \begin{pmatrix} \pi_{11} & \pi_{12} \\ \pi_{21} & \pi_{22} \end{pmatrix}$ in 2×2 games [31]. Thus, the expected payoffs in the BOS are: $\begin{matrix} p_{♂} = \pi_{11} R + \pi_{22} r \\ p_{♀} = \pi_{11} r + \pi_{22} R \end{matrix}$. If $\pi_{11} = \pi_{22} = \pi$, both players get the same payoff $p^= = \pi(R + r)$. So that if $\pi > 1/4$ the players get equalitarian payoffs that are not accessible in the uncorrelated strategies scenario, with maximum $p^+ = (R + r)/2$ if $\pi = 1/2$.

The quantum game approach, described in the next subsection, includes both the independent players model (1), and the correlated games ruled by $\mathbf{\Pi}$.

2.2 Quantum games

In the quantization scheme introduced by Eisert et al. [14] (EWL henceforth), the classical pure strategies are assigned two basic vectors $|0\rangle$ and $|1\rangle$, respectively, in a two-level Hilbert space. The state of the game is a vector in the tensor product space spanned by the basis vectors $|00\rangle$, $|01\rangle$, $|10\rangle$, $|11\rangle$, where the first and second entries in the ket refers to the players A and B, respectively.

The EWL protocol starts with an initial entangled state $|\psi_i\rangle = \hat{J}|00\rangle$, where $\hat{J}$ is a symmetric unitary operator that *entangles* the players qubits and that is known to both players. $\hat{J}$ is chosen so that the classical game is a subset of its quantum version as $\hat{J} = \exp\left(i\frac{\gamma}{2}\hat{D}^{\otimes 2}\right)$, where the *entanglement factor* $\gamma \in [0, \pi/2]$ tunes the degree of entanglement achieved by $\hat{J}(\gamma)$.

The players chose independently their quantum strategies as local unitary operators $\hat{U}_A$ and $\hat{U}_B$. After the application of these strategies, the state of the game evolves to $|\psi_{f_o}\rangle = (\hat{U}_A \otimes \hat{U}_B)\hat{J}|00\rangle$. Prior to measurement, the $\hat{J}^\dagger$ gate is applied and the state of the game becomes:

$$|\psi_f\rangle = \hat{J}^\dagger(\hat{U}_A \otimes \hat{U}_B)\hat{J}|00\rangle \equiv (\psi_1\psi_2\psi_3\psi_4)^{'} \tag{2}$$

This follows a pair of Stern–Gerlach-type detectors for measurement. As a result,

$$\mathbf{\Pi} = \begin{pmatrix} |\psi_1|^2 & |\psi_2|^2 \\ |\psi_3|^2 & |\psi_4|^2 \end{pmatrix} \tag{3}$$

Consequently, the expected payoffs in the BOS become:

$$p_{\left\{\begin{smallmatrix}\male\\ \female\end{smallmatrix}\right\}} = \left\{\begin{matrix} R \\ r \end{matrix}\right\} |\psi_1|^2 + \left\{\begin{matrix} r \\ R \end{matrix}\right\} |\psi_4|^2 \tag{4}$$

We will considerer here the two-parameter (2P) subset of the SU(2) space of strategies:

$$\hat{U}(\theta, \alpha) = \begin{pmatrix} e^{i\alpha}\cos(\theta/2) & \sin(\theta/2) \\ -\sin(\theta/2) & e^{-i\alpha}\cos(\theta/2) \end{pmatrix}, \qquad \begin{matrix} \theta \in [0, \pi] \\ \alpha \in [0, \pi/2] \end{matrix}. \tag{5}$$

If α_A=$\alpha_B = 0$, or if $\gamma = 0$, Π factorizes as in the *classical* uncorrelated game (1) using $x = \cos^2(\theta_A/2)$, $y = \cos^2(\theta_B/2)$. So to say, the θ parameters are the *classical* ones. In the classic $\gamma = 0$ context, middle levels of the (θ,α) parameters lead to equal probabilities in $\mathbf{\Pi}$, so, in the BOS: $p_{\male} = p_{\female} = (R + r)/4$.

In contrast, with maximal entangling ($\gamma = \pi/2$), if θ_A=θ_B=0, $\mathbf{\Pi}$ becomes diagonal, i.e. non-factorizable, with: $\pi_{11} = \cos^2(\alpha_A + \alpha_B)$, $\pi_{22} = 1 - \pi_{11}$. With $\gamma = \pi/2$

and middle-level parameter values, $\mathbf{\Pi}$ degenerates, as $\boldsymbol{\pi}_{22} = 1$. Thus, the 2P model is somehow biased towards the female player.

We will consider here also the three-parameter strategies (3P) scenario [7]:

$$\hat{U}(\theta, \alpha, \beta) = \begin{pmatrix} e^{i\alpha}\cos(\theta/2) & e^{i\beta}\sin(\theta/2) \\ -e^{-i\beta}\sin(\theta/2) & e^{-i\alpha}\cos(\theta/2) \end{pmatrix}, \qquad \begin{matrix} \theta \in [0, \pi] \\ \alpha, \beta \in [0, \pi/2] \end{matrix}. \tag{6}$$

3 Imperfect information

Let us suppose that the male player is unsecure whether the female player prefers to join him or prefers to avoid him. He believes that the two ♀-types deserve the probabilities $\left(\lambda_{♂}, 1 - \lambda_{♂}\right)$ [18,36]. In such as scenario, the payoff matrices of the two ♀-types are given in Fig. 1.

If neither player knows whether the other wants to meet on not, with the male player assigning $(\lambda_{♂}, 1 - \lambda_{♂})$, and the female assigning the probabilities $(\lambda_{♀}, 1 - \lambda_{♀})$, the payoff matrices are given in Fig. 2.

A general assignment of probabilities in the scenario of Fig. 2 is shown in Fig. 3.

The layout probabilities given in Fig. 3 together with the belief probabilities generate the expected payoffs in the BOS:

Fig. 1 Payoff matrices for an unsecure male player

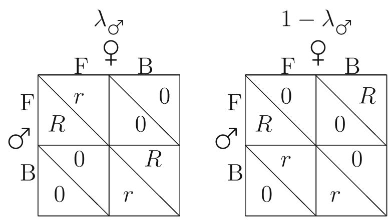

Fig. 2 Payoff matrices in an imperfect information BOS game

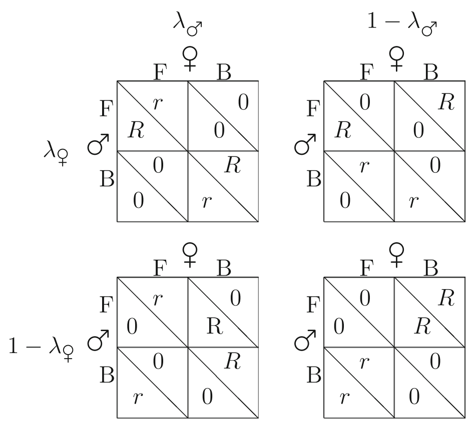

Fig. 3 A general assignment of probabilities in the scenario of Fig. 2

		♀1		♀2	
♂1		ϵ_1	ϵ_2	ϵ_5	ϵ_6
		ϵ_3	ϵ_4	ϵ_7	ϵ_8
♂2		ϵ_9	ϵ_{10}	ϵ_{13}	ϵ_{14}
		ϵ_{11}	ϵ_{12}	ϵ_{15}	ϵ_{16}

$$\begin{aligned}
p_{\male_1} &= \lambda_{\male}\big(R\epsilon_1 + 0\epsilon_2 + 0\epsilon_3 + r\epsilon_4\big) + (1-\lambda_{\male})\big(R\epsilon_5 + 0\epsilon_6 + 0\epsilon_7 + r\epsilon_8\big)\\
p_{\male_2} &= \lambda_{\male}\big(0\epsilon_9 + R\epsilon_{10} + r\epsilon_{11} + 0\epsilon_{12}\big) + (1-\lambda_{\male})\big(0\epsilon_{13} + R\epsilon_{14} + r\epsilon_{15} + 0\epsilon_{16}\big)\\
p_{\female_1} &= \lambda_{\female}\big(r\epsilon_1 + 0\epsilon_2 + 0\epsilon_3 + R\epsilon_4\big) + (1-\lambda_{\female})\big(r\epsilon_9 + 0\epsilon_{10} + 0\epsilon_{11} + R\epsilon_{12}\big)\\
p_{\female_2} &= \lambda_{\female}\big(0\epsilon_5 + R\epsilon_6 + r\epsilon_7 + 0\epsilon_8\big) + (1-\lambda_{\female})\big(0\epsilon_{13} + R\epsilon_{14} + r\epsilon_{15} + 0\epsilon_{16}\big)
\end{aligned} \tag{7}$$

The probabilities in Fig. 3 must obey to the normalization constraints: $\sum_{i=1}^{4}\epsilon_i = \sum_{i=5}^{8}\epsilon_i = \sum_{i=9}^{12}\epsilon_i = \sum_{i=13}^{16}\epsilon_i = 1$, and in the EPR experiment inspired approach followed in [18] also to the locality constraints: $\epsilon_1+\epsilon_2 = \epsilon_5+\epsilon_6, \epsilon_3+\epsilon_4 = \epsilon_7+\epsilon_8$; $\epsilon_9+\epsilon_{10} = \epsilon_{13}+\epsilon_{14}$; $\epsilon_{11}+\epsilon_{12} = \epsilon_{15}+\epsilon_{16}$; $\epsilon_1+\epsilon_3 = \epsilon_9+\epsilon_{11}$; $\epsilon_2+\epsilon_4 = \epsilon_{10}+\epsilon_{12}$; $\epsilon_5+\epsilon_7 = \epsilon_{13}+\epsilon_{15}$; $\epsilon_6+\epsilon_8 = \epsilon_{14}+\epsilon_{16}$.

At variance with the general procedure of constructing the layout of ϵ-probabilities adopted in [18], in this work every submatrix in Fig. 3 will be equalized to Π, thus:

$$\begin{pmatrix}\epsilon_1 & \epsilon_2\\ \epsilon_3 & \epsilon_4\end{pmatrix} = \begin{pmatrix}\epsilon_5 & \epsilon_6\\ \epsilon_7 & \epsilon_8\end{pmatrix} = \begin{pmatrix}\epsilon_9 & \epsilon_{10}\\ \epsilon_{11} & \epsilon_{12}\end{pmatrix} = \begin{pmatrix}\epsilon_{13} & \epsilon_{14}\\ \epsilon_{15} & \epsilon_{16}\end{pmatrix} = \mathbf{\Pi} = \begin{pmatrix}\pi_{11} & \pi_{12}\\ \pi_{21} & \pi_{22}\end{pmatrix} \tag{8}$$

Consequently,

$$\begin{aligned}
p_{\male_1} &= \lambda_{\male}\big(R\pi_{11} + r\pi_{22}\big) + (1-\lambda_{\male})\big(R\pi_{11} + r\pi_{22}\big) = R\pi_{11} + r\pi_{22}\\
p_{\male_2} &= \lambda_{\male}\big(R\pi_{12} + r\pi_{21}\big) + (1-\lambda_{\male})\big(R\pi_{12} + r\pi_{21}\big) = R\pi_{12} + r\pi_{21}\\
p_{\female_1} &= \lambda_{\female}\big(r\pi_{11} + R\pi_{22}\big) + (1-\lambda_{\female})\big(r\pi_{11} + R\pi_{22}\big) = r\pi_{11} + R\pi_{22}\\
p_{\female_2} &= \lambda_{\female}\big(R\pi_{12} + r\pi_{21}\big) + (1-\lambda_{\female})\big(R\pi_{12} + r\pi_{21}\big) = R\pi_{12} + r\pi_{21}
\end{aligned} \tag{9}$$

Please note in (9) that $p_{\male_2} = p_{\female_2}$.

In this study, every male/female player will be featured by a sole payoff constructed as:

$$\begin{aligned}
p_{\male} &= \lambda_{\female}\, p_{\male_1} + \big(1-\lambda_{\female}\big)\, p_{\male_2}\\
p_{\female} &= \lambda_{\male}\, p_{\female_2} + \big(1-\lambda_{\male}\big)\, p_{\female_2}
\end{aligned} \tag{10}$$

4 The spatialized QBOS

In the spatial version of the BOS we deal with, each player occupies a site (i, j) in a two-dimensional $N \times N$ lattice. We will consider that *males* and *females* alternate

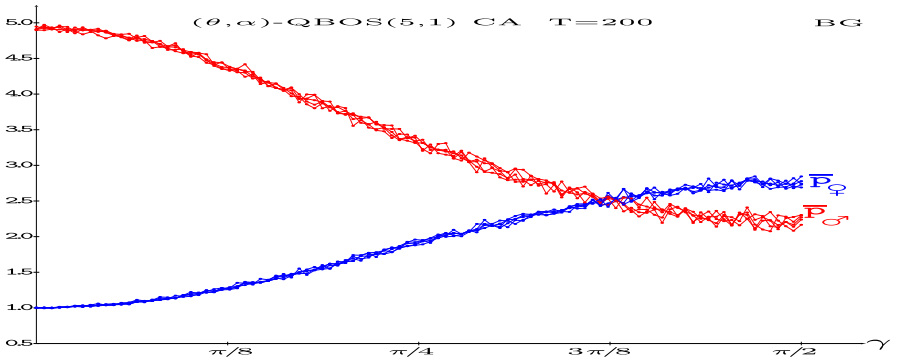

Fig. 4 Long-term mean payoffs in five simulations of a two-parameter (5,1)-QBOS–CA with entangling factor γ. Imperfect information in both the male (*red-marked*), and the female (*blue-marked*) players (Color figure online)

in the site occupation. Thus, both kind of players are arranged in a chessboard form, so that every player is surrounded by four partners (♀ − ♂, ♂ − ♀), and four mates (♀ − ♀, ♂ − ♂).

In a cellular automata (CA)-like implementation of the players' interaction, in each generation (T) every player plays with his four adjacent partners, so that the payoff $p_{i,j}^{(T)}$ of a given individual is the sum over these four interactions, each of them generating payoffs according to (10). In the next generation, every player will adopt the quantum parameters $\left(\alpha_{i,j}^{(T)}, \theta_{i,j}^{(T)}\right)$ and the belief probability $\lambda_{i,j}^{(T)}$ of his nearest-neighbour mate (including himself) that received the highest payoff.

Details of the *male–female* site occupation, as well as simple examples of the initial dynamics in the perfect information scenario are given in [3–5]. Incidentally, studies of the spatialized quantum prisoner's dilemma with perfect information have been reported in [1,2].

All the simulations in this work are run in a $N = 200$ lattice with periodic boundary conditions and initial random assignment of the quantum parameters and belief probabilities. Thus, initially: $\overline{\lambda} \simeq 1/2$, and $\overline{\theta} \simeq \pi/2 = 1.57$, $\overline{\alpha} \simeq \pi/4 = 0.78$. The computations have been performed by a double precision Fortran code run on a mainframe.

Figure 4 shows the long-term payoffs in five simulations of a two-parameter (5,1)-QBOS–CA with variable entanglement factor γ. It is remarkable that for any given value of γ, the variation of the initial parameter pattern configurations only alters minor details of the evolving dynamics, the main features of the dynamics and of the long-term patterns are preserved.

The bias towards the female player in the model with maximal entangling (pointed out in the Introduction Sect. 2.2) becomes apparent in Fig. 4 for high γ values, specifically for $\gamma > 3\pi/8$. In contrast to this, with $\gamma < 3\pi/8$ the male player overrates the female player, in a dramatic way for low values of γ, with the extreme scenario for the classic $\gamma = 0$ in which case $\overline{p}_{♂} = 5$, $\overline{p}_{♀} = 1$. The behaviour for low values of γ notably differs from this one in the perfect information scenario (as shown in Fig. 1 in [3]), where: (i) both mean payoffs are similar close to $\gamma = 0$, (ii) the initial increase

in γ leads to a dramatic bifurcation in favour of the male player reaching a peak close to (5,1) when γ approaches $\pi/8$, and (iii) before, but close, this value of γ, both mean payoffs approach as γ increases, reaching fairly equal values by $\gamma \simeq 3\pi/8$, much in as similar way as in the imperfect information scenario studied here.

Figure 5 shows the dynamics of the mean probabilities in Π and the mean belief probabilities in a simulation of Fig. 4 up to $T = 20$. In the left panel, as $\gamma = 0.0$ it is initially $\overline{\pi}_{11} \simeq \overline{\pi}_{12} \simeq \overline{\pi}_{21} \simeq \overline{\pi}_{22} \simeq 1/4$. In the right panel, with maximum entangling, the highest initial $\overline{\pi}$ is $\overline{\pi}_{22}$ and the lowest is $\overline{\pi}_{11}$, accordingly to the bias to the female player in the 2P-model. In the $\gamma = 0.0$ scenario (left panel), $\overline{\pi}_{11}$ notably increases its value in the evolving dynamics, whereas the remaining $\overline{\pi}$ values plummet to zero, what supports the distant $\overline{p}_{\male} = 5$, $\overline{p}_{\female} = 1$ payoffs for $\gamma = 0$ in Fig. 4. In the $\gamma = \pi/2$ scenario (right panel), $\overline{\pi}_{22}$ remains over $\overline{\pi}_{11}$ in the evolving dynamics, though approaching their values (at $T = 200$ it is $\overline{\pi}_{11} = 0.381$, $\overline{\pi}_{22} = 0.555$), which explains why $\overline{p}_{\female}$ overrates $\overline{p}_{\male}$ for $\gamma = \pi/2$ in Fig. 4, albeit not in a great extent. Further evolution of the simulation treated in the right panel of Fig. 5 is shown in Fig. 6.

The evolution of the mean belief probabilities in Fig. 5 is highly remarkable. In the untangled scenario (left), both $\overline{\lambda}$ parameter values rocket towards 1.0 from its initial 0.5 random assignment, in the fully entangled (right) the drift to 1.0 is also very noticeable, albeit not so dramatic as in the unentangled model and showing a small lag in both $\overline{\lambda}$ values. The drift to 1.0 of the beliefs of both types of players becomes a key feature in the simulations in this study (see also Figs. 12, 13 at this respect).

The long-term dynamics in the scenario of Fig. 4 whose initial dynamics is shown in the right panel of Fig. 5, i.e. dealing with maximum $\gamma = \pi/2$, is shown in Fig. 6. The far left panel of the figure shows the evolution up to $T = 200$ of the mean values across the lattice of (θ, α) as well of the actual $(\overline{\boldsymbol{p}})$ mean payoffs. The $\overline{\theta}$ values evolve initially in opposite direction from their mean values, close to $\pi/2 = 1.57$, a $\overline{\theta}_{\male}$ decreases, whereas $\overline{\theta}_{\female}$ grows, but the ulterior dynamics depletes the $\overline{\theta}_{\female}$ value, so that both $\overline{\theta}$ parameter values decrease slowly in a fairly parallel extent, and at $T = 200$ it is $\overline{\theta}_{\female} = 0.64$; $\overline{\theta}_{\male} = 0.36$. The dynamics of both $\overline{\alpha}$ parameter values is smoother compared with that of $\overline{\theta}$, so from the initial $\overline{\alpha} \simeq \pi/4 = 0.78$, at $T = 200$ it is: $\overline{\alpha}_{\male} = 0.81 \simeq \overline{\alpha}_{\female} = 0.82$. The parameter dynamics in Fig. 6 quickly drives the $\overline{\boldsymbol{p}}$ mean payoffs to distant values, so that from approximately $T = 100$ they become fairly stabilized, reaching at $T = 200$ the values: $\overline{\boldsymbol{p}}_{\female} = 2.80$, $\overline{\boldsymbol{p}}_{\male} = 2.14$.

Figure 6 shows also the snapshots of the parameter and payoff patterns at $T = 200$, both for the full lattice and its zoomed 23×23 central part. Rich maze-like structures may be appreciated in the parameter patterns, particularly in the α parameter pattern, whereas in the θ and payoff patterns, the maze-like structure appears fairly fuzzyfied.

The spatial heterogeneity in the parameter values difficult the capacity of the mean-field payoff estimations computed as proposed in Sect. 6 to approach the actual mean payoffs. Maze-like structures in the parameter patterns emerge as soon as γ takes off, and consequently, the mean-field p^* values tend to poorly reflect the actual mean payoffs of both kinds of players as γ grows (see Fig. 12).

Figure 7 shows the asymptotic payoffs in the scenario of Fig. 4, but in the three-parameter strategies model. The plots in both figures notably resemble, though in the

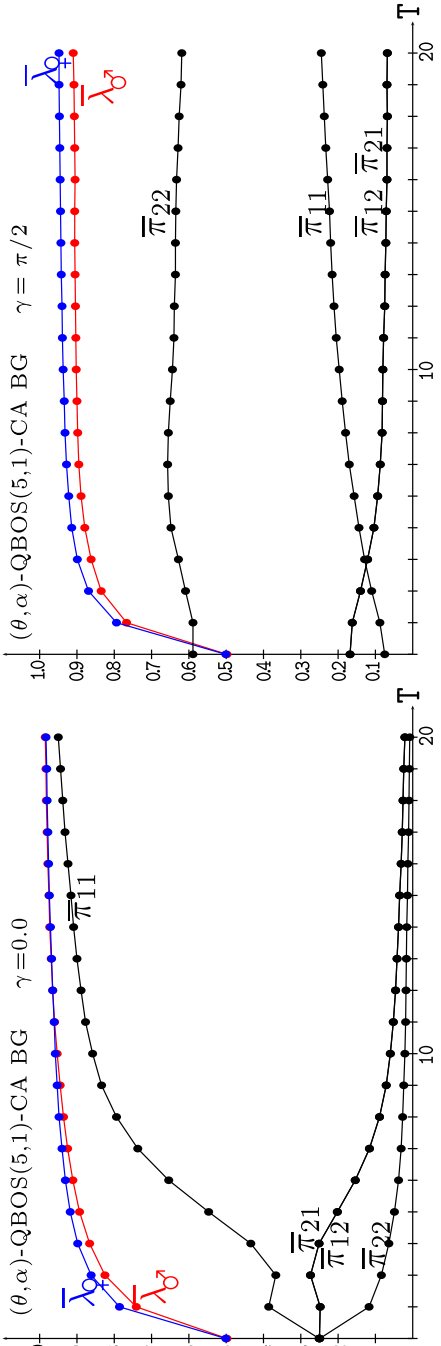

Fig. 5 Dynamics of the mean probabilities in Π and the mean belief probabilities in a simulation of Fig. 4 up to $T = 20$. *Left* $\gamma = 0.0$. *Right* $\gamma = \pi/2$

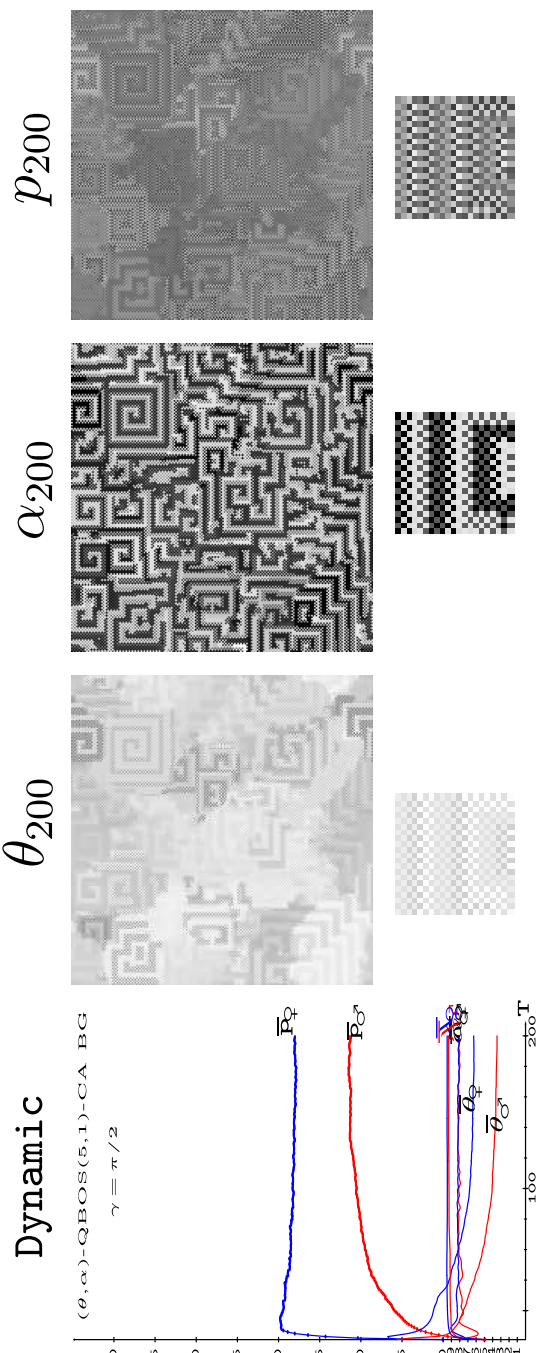

Fig. 6 Simulation of a 2P (5,1)-QBOS–CA in the scenario of Fig. 4 with $\gamma = \pi/2$. *Far left* evolving mean parameters and payoffs. *Centre* parameter patterns at $T = 200$. *Far right* payoff pattern at $T = 200$. Increasing *grey levels* indicate increasing parameter pattern values

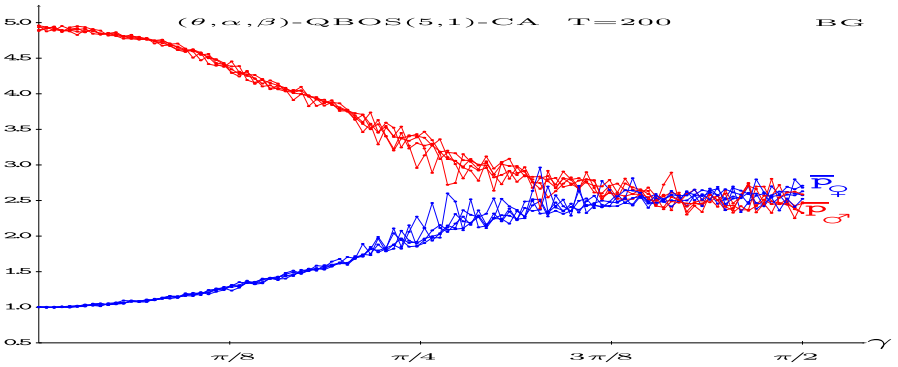

Fig. 7 Long-term mean payoffs in five simulations of a three-parameter (5,1)-QBOS–CA with entangling factor γ. Imperfect information in both the male (*red-marked*) and the female (*blue-marked*) players (Color figure online)

3P model, there is not any bias favouring the female player, not even for high values of the entangling factor (as shown in Fig. 4), so that for $\gamma > 3\pi/8$ both mean payoffs are not significantly different.

The parameter patterns show also in the 3P model a rich maze-like structure as soon as γ takes off, similarly to what happens in the 2P model, i.e. particularly in the case of the α patterns and now also regarding the β patterns.

At variance with what happens with imperfect information here, in the 3P with perfect information (Fig. 4 in [3]), the mean payoffs are not dramatically altered by the variation of γ. The overall effect of the increase in γ being a moderation in the variation of the $\overline{p}$ values that oscillate nearly over 2.5.

Please recall from the Introduction section that the maximum equalitarian payoff in the uncorrelated context is $p^+ = (R + r)/4 = 1.5$, whereas the mean payoffs in the simulations of a three-parameter (5,1)-QBOS–CA with high entanglement factor in Fig. 7 reach values over 2.5, not far from the maximum feasible equalitarian payoff $p^= = (R + r)/2 = 3.0$.

The main features of the plots in the Figs. 4 and 7 have been checked to be preserved with the BOS parameters (2,1), (4,1) and (6,1). In these three cases, the general form of the $\overline{\boldsymbol{p}}$ versus γ plots is that shown here for (5,1), reaching long-term $\overline{\boldsymbol{p}}$ values not far from $(R + r)/2$. Thus, with $R = 2$ around 1.5, with $R = 4$ around 2.25, and with $R = 6$ around 3.25.

5 Unfair contests

Let us assume the unfair situation: A type of players is restricted to classical strategies $\tilde{U}(\theta, 0)$, whereas the other type of players may use quantum $\hat{U}(\theta, \alpha)$ ones [15].

Figure 8 shows the asymptotic payoffs in five simulations of an unfair two-parameter quantum versus classic players in a (5,1)-BOS–CA with variable entanglement factor γ. The case of the quantum male (red) versus classic female (blue), shown in the left panel, behaves as expected a priori: the quantum player overrates the classic one. That

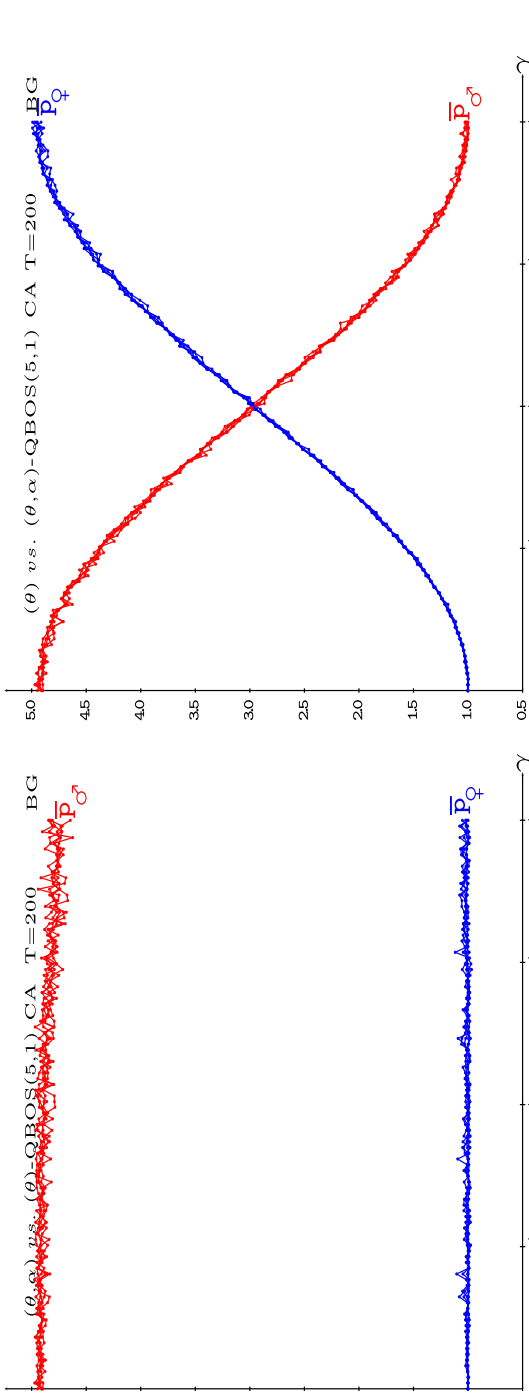

Fig. 8 Long-term payoffs in five simulations of a 2P-quantum versus classic (5,1)-BOS–CA with entanglement factor γ. *Left* quantum male (*red*) versus classic female (*blue*). *Right* classic male (*red*) versus quantum female (*blue*) (Color figure online)

is so in an extreme way, $\overline{p}_{\male} = 5$, $\overline{p}_{\female} = 1$, regardless the γ parameter value. At variance with this, the case of the classic male (red) versus quantum female (blue), shown in the right panel, shows a dramatic dependence of the γ: the classic male overrates the quantum female for $\gamma < \pi/2$, where the opposite ordering of payoffs (that expected a priori) appears for $\gamma > \pi/2$,

The parameter patterns in the scenarios of Fig. 8 are free of spatial effects, so that the mean-field approximation operates fairly well. Thus, in the left panel the (θ, α) parameters approach to zero in the long-term, so that π^*_{11} approach to 1.0, and consequently $p^*_{\male} \simeq R = 5$, $p^*_{\female} \simeq r = 1$, in agreement with the graphs of the actual mean payoffs. The *scissors*-like form of the graphs emerging in the right panel of Fig. 8 will be commented in Sect. 6.

Figure 9 shows the asymptotic payoffs in five simulations of an unfair three-parameter quantum versus classic players in a (5,1)-BOS–CA with variable entanglement factor γ. The graphs in the right panel of Fig. 9 (classic male vs. quantum female) are similar to those in the same scenario with two parameters shown in the right panel of Fig. 8. At variance with this, the graphs in the left panel of Fig. 9 (quantum male vs. classic female) shows that the advantage of the quantum male in the 3P scenario is not as evident as in the 2P case (left panel of Fig. 9). This advantage appears notably weakened circa the middle $\gamma = \pi/4$, with the semi-quantum female overrating the full quantum male in the proximity of this value.

Figures 10 and 11 consider the case of three-parameter quantum versus semi-quantum contests, semi-quantum referring to players that may not implement one of the *quantum* parameters, either α or β, but have access to the other one, β or α, respectively (in both cases with the θ parameter operative). Let us remark first that these figures reveal that the roles of the α and β parameters in the three-parameter model are fairly different.

The aspect of the graphs in Figs. 10 and 11 is roughly comparable to those in Fig. 9. Thus, in the left panels the advantage of the full quantum male decreases as γ grows up to approximately $\gamma = \pi/4$; then, it is recovered after this value of the entanglement factor, though in a different way Figs. 10 and 11 compared with the robust way shown in Fig. 9. The *scissors*-like form of the graphs in the right panel of Fig. 9 is much altered in Figs. 10 and 11. It is also remarkable that the graphs in Fig. 11 show a noisy aspect for high γ values which is not found in the other plots in this study.

6 Mean-field approach

Mean-field payoffs may be computed in a single hypothetical two-person game with players adopting the mean parameters appearing in the spatial dynamic simulation. Thus, from $U^*_{\male}(\overline{\theta}_{\male}, \overline{\alpha}_{\male})$, $U^*_{\female}(\overline{\theta}_{\female}, \overline{\alpha}_{\female})$, the joint probability distribution Π^* is calculated according to (3); then, the payoffs $p^*_{\male_1}$, $p^*_{\male_2}$, $p^*_{\female_1}$, $p^*_{\female_2}$ are to be computed according to (9) using the probabilities in Π^*, and finally

$$\begin{aligned} p^*_{\male} &= \overline{\lambda}_{\female} p^*_{\male_1} + (1 - \overline{\lambda}_{\female}) p^*_{\male_2} \\ p^*_{\female} &= \overline{\lambda}_{\male} p^*_{\female_2} + (1 - \overline{\lambda}_{\male}) p^*_{\female_2} \end{aligned} \tag{11}$$

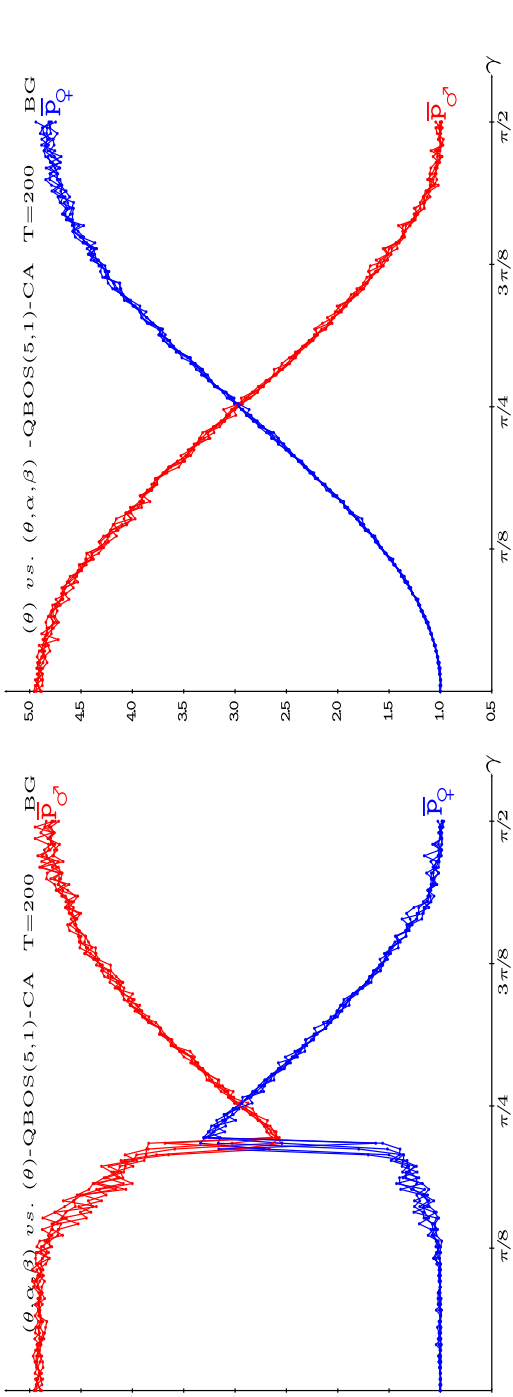

Fig. 9 Long-term payoffs in five simulations of a three-parameter quantum versus classic (5,1)-BOS–CA with entanglement factor γ. *Left* quantum male versus classic female. *Right* classic male versus quantum female

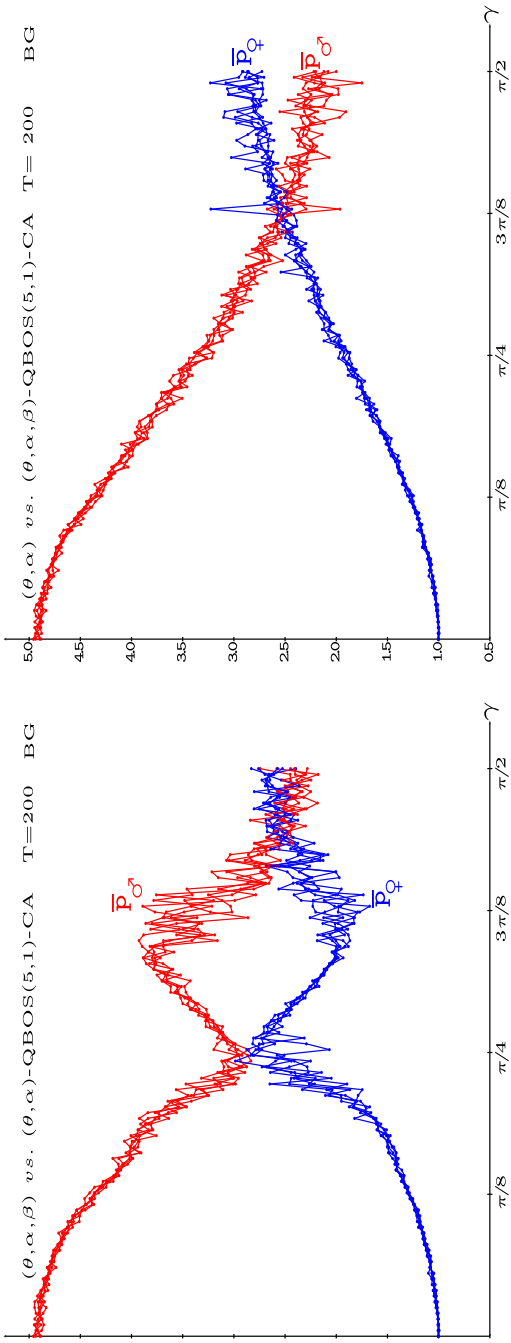

Fig. 10 Long-term payoffs in five simulations of (θ, α, β) versus (θ, α) players in a (5,1)-BOS–CA with entanglement factor γ. *Left* quantum male versus semi-quantum female. *Right* semi-quantum male versus quantum female

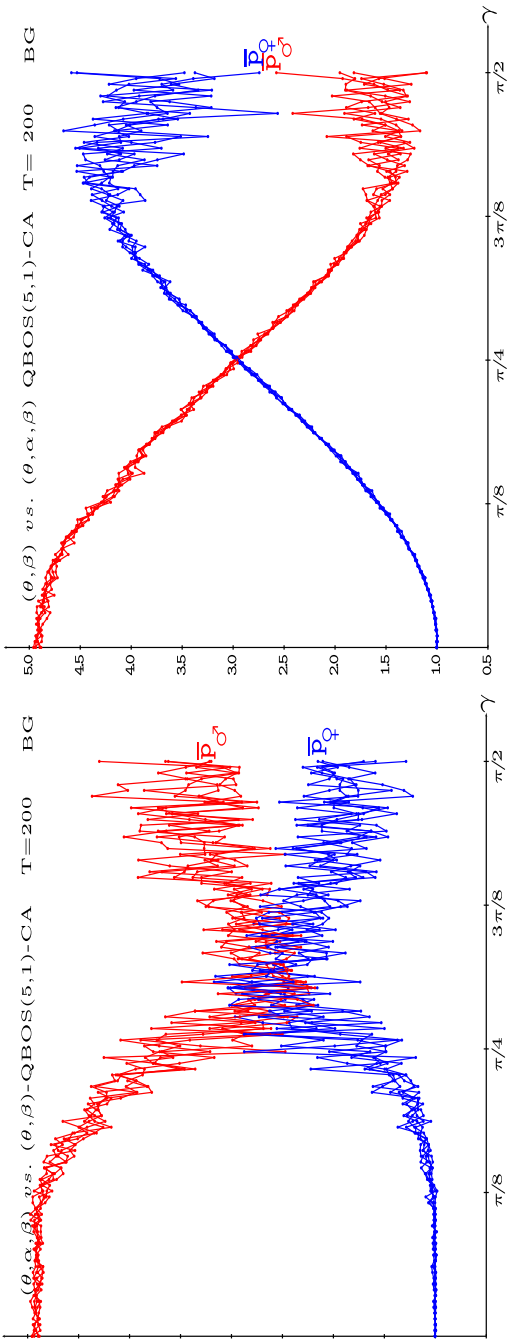

Fig. 11 Long-term payoffs in five simulations of (θ, α, β) vs. (θ, β) players in a (5,1)-BOS–CA with entanglement factor γ. *Left* quantum male versus semi-quantum female. *Right* semi-quantum male versus quantum female

Figure 12 shows the long-term mean parameters (left panel) and the actual ($\overline{p}$) and mean-field (p^*) payoffs (right panel) computed according to (11) in the 2P-(5,1)-QBOS–CA scenario of Fig. 4. Spatial effects are in the origin of the divergence of the actual mean payoffs and their mean-field approximation. The divergence increases as γ increases, as the values of both types of actual payoffs are approached compared with their corresponding mean-field approximations. The same effect operates in the scenario of Fig. 7.

Figure 13 shows the long-term mean parameters (left panel) and the mean-field payoffs (right panel) computed according to (11) in the unfair 2P scenario of the right panel of Fig. 8. The absence of spatial effects in this scenario explains why the mean-field approximation fits almost perfectly to the actual mean payoffs.

In the conventional (non-CA) 2P-EWL quantum model with perfect information (3), the diagonal elements of $\mathbf{\Pi}$ are (with ω standing for $\theta/2$):

$$\begin{aligned} |\psi_1|^2 &= \cos^2\omega_{\male}\cos^2\omega_{\female}\left(\cos^2\gamma\sin^2\left(\alpha_{\male}+\alpha_{\female}\right)+\cos^2\left(\alpha_{\male}+\alpha_{\female}\right)\right) \\ |\psi_4|^2 &= \left(\sin\gamma\cos\omega_{\male}\cos\omega_{\female}\sin(\alpha_{\male}+\alpha_{\female})+\sin\omega_{\male}\sin\omega_{\female}\right)^2 \end{aligned} \tag{12}$$

Which if $\alpha_{\male}+\alpha_{\female}=\pi/2$ reduces to:

$$\begin{aligned} |\psi_1|^2 &= \cos^2\omega_{\male}\cos^2\omega_{\female}\cos^2\gamma \\ |\psi_4|^2 &= (\sin\gamma\cos\omega_{\male}\cos\omega_{\female}+\sin\omega_{\male}\sin\omega_{\female})^2 \end{aligned} \tag{13}$$

Equations (13) simplifies to the below equations (14) if also $\theta_{\male}=\theta_{\female}=0$:

$$\begin{aligned} |\psi_1|^2 &= \cos^2\gamma \\ |\psi_4|^2 &= \sin^2\gamma \end{aligned} \tag{14}$$

In the scenario of equations (14) it is:

$$p_{\left\{\begin{smallmatrix}\male\\ \female\end{smallmatrix}\right\}} = \left\{\begin{matrix}R\\ r\end{matrix}\right\}\cos^2\gamma+\left\{\begin{matrix}r\\ R\end{matrix}\right\}\sin^2\gamma \tag{15}$$

The drift to 1.0 of the beliefs of both types of players found in this study, revealed in particular in the left panels of Figs. 12 and 13, allows considering the just above formulas obtained in the conventional (non-CA) 2P-EWL perfect information context to explain the mean-field approximations.

Equation (15) generates the kind of *scissors* shape found in some graphs in this work. Thus, for example: *i*) in the scenario of Fig. 13, where (left panel) $\overline{\alpha}_{\male}=0$, $\overline{\alpha}_{\female}\simeq\pi/2$, and both values of $\overline{\theta}$ are low, and *ii*) in the scenario of Fig. 12, where (left panel) $\overline{\alpha}_{\male}\simeq\overline{\alpha}_{\female}\simeq\pi/4$, and both values of $\overline{\theta}$ are not high. Please recall that $\theta\in[0,\pi]$ and that in (12) it is $\omega\equiv\theta/2$. It is remarkable that in the full entangling 2P-EWL model, strategies with $\alpha_{\male}+\alpha_{\female}=\pi/2$ and $\theta_{\male}=\theta_{\female}=0$ are in Nash equilibrium [12,13].

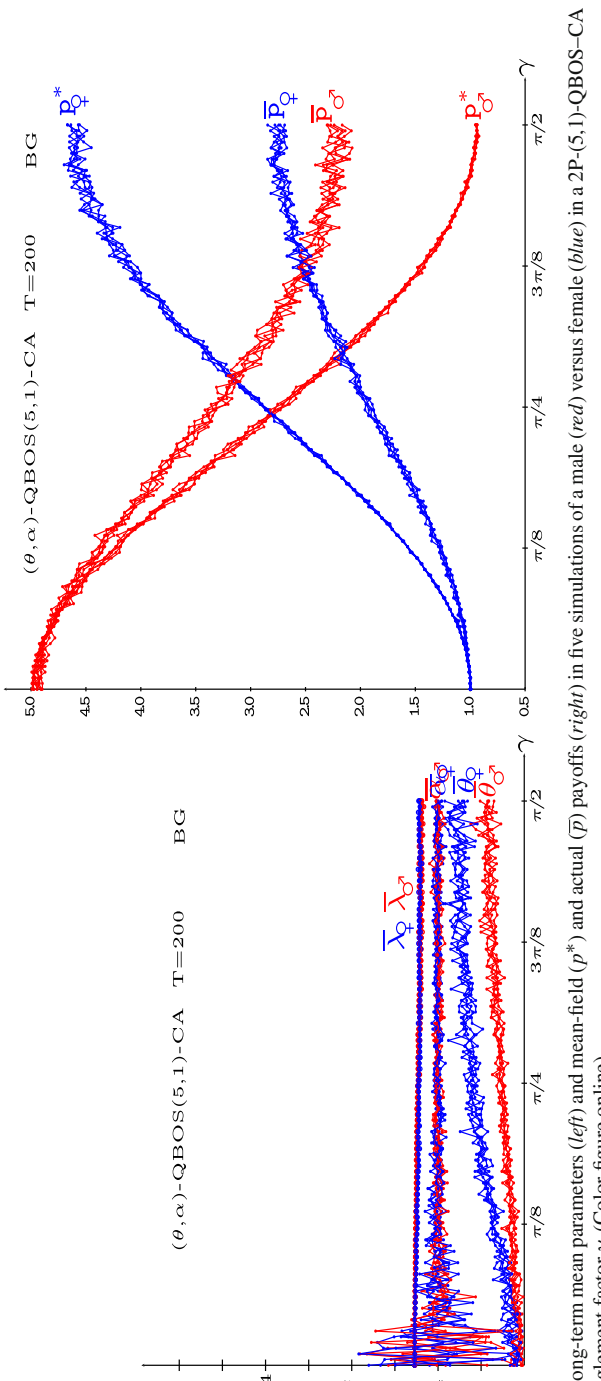

Fig. 12 Long-term mean parameters (*left*) and mean-field (p^*) and actual ($\overline{p}$) payoffs (*right*) in five simulations of a male (*red*) versus female (*blue*) in a 2P-(5,1)-QBOS–CA with entanglement factor γ (Color figure online)

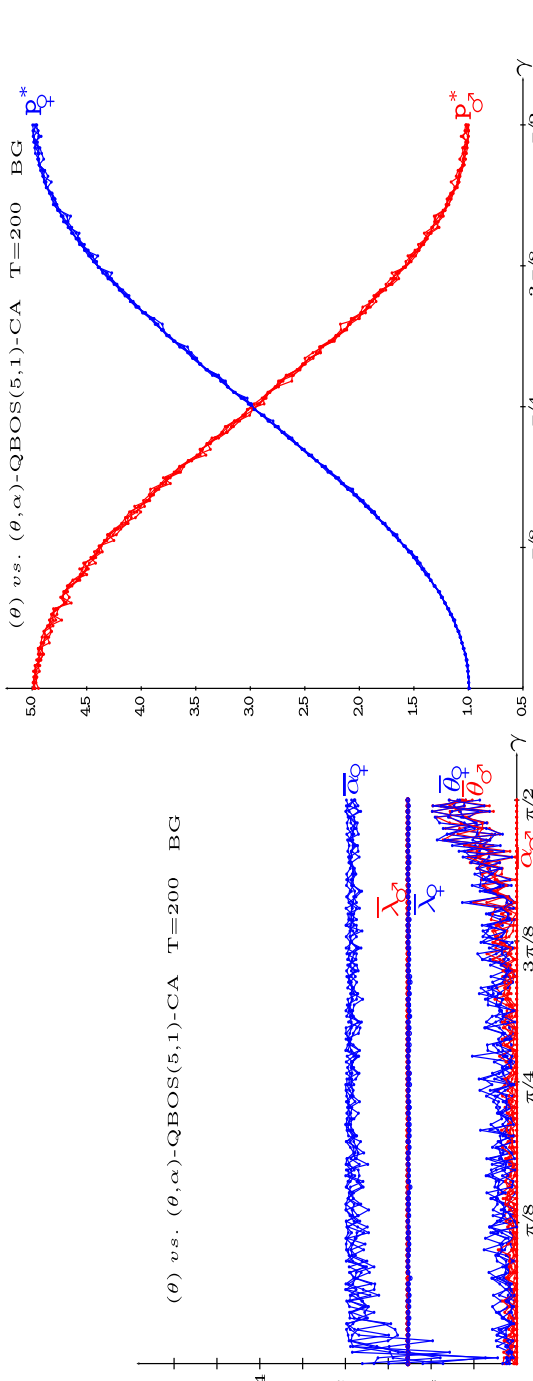

Fig. 13 Long-term mean parameters (*left*) and mean-field payoffs (*right*) in five simulations of a two-parameter quantum female (*blue*) versus classic male (*red*) in a (5,1)-BOS–CA with entanglement factor γ (Color figure online)

7 Conclusions and future work

The dynamics of a spatial quantum formulation of the iterated battle of the sexes (BOS) game with imperfect information is studied in this work. The game is played with variable entangling in a cellular automata (CA) manner, i.e. with local and synchronous interaction among players. The evolution is guided by the imitation of the best paid neighbour.

The main finding reported in this work is that of the recovering of the perfect information scenario in the CA-dynamics, i.e. the original formulation of the BOS game, in which coordination is desirable. But the transition from a random assignment of beliefs into the belief in what both players want to meet the other induces quantum parameter and payoff patterns that notably differ from those achieved dealing with the perfect information QBOS–CA game [3].

The intrinsic asymmetry of the BOS game induces a very interesting modification in the payoffs that the players achieve when varying the correlation of the player's strategies, i.e. the entangling factor γ. The effect of the variation of this parameter has been studied considering quantum models with two and three free parameters, and in fair (both players allowed implementing quantum strategies) and unfair (one of the players remains classic) scenarios.

The results reported in this article apply precisely for the case of the ($R = 5, r = 1$) BOS parameters, but they have been checked to qualitatively apply for more separated parameter values, such as (6,1), and with close numerical values such as (2,1). An analytical study of cellular automaton quantum games with imperfect information is due, albeit it appears to be very challenging.

Further study is due on games with asynchronous and probabilistic CA-updating, as well as on the effect of increasing degrees of spatial dismantling, and that of memory [6]. These are deviations from the canonical cellular automata paradigm which may lead to more realistic models.

This study adopts one of the possible quantization schemes (that referred to as EWL in the specialized literature). Other quantization schemes [19,20,28,29] deserve to be studied in the spatial context. In particular, the scheme introduced by Marinatto and Weber [25,35], a model with no bias favouring to any of the players.

Last but not least, the BOS and other games, e.g. the prisoner's Dilemma, with imperfect information embedded in a cellular automaton are to be studied when assigning joint probabilities inspired in the EPR experiment [10,18].

Quantum game theory occupies a somewhat peculiar position among the quantum information processing lines of research. This is so at a great extent because the usual applications of game theory—sociology, economics, evolutionary biology—are not, so far, in the realm of quantum mechanics. But the game strategies residing on qubit space have intricacies that deserve to be uncovered. This article aims to contribute to this goal, by considering the added component of player's spacialization.

Acknowledgments This work was supported by the Spanish Grant M2012-39101-C02-01. Part of the computations were performed in the HPC machines EOLO and FISWULF, based on the International Campus of Excellence of Moncloa, funded by the Spanish Government and Feder funds.

References

1. Alonso-Sanz, R.: Variable entangling in a quantum prisoner's dilemma cellular automaton. Quantum Inf. Process. **14**(1), 147–164 (2015)
2. Alonso-Sanz, R.: A quantum prisoner's dilemma cellular automaton. Proc. R. Soc. A **470**, 20130793 (2014)
3. Alonso-Sanz, R.: Variable entangling in a quantum battle of the sexes cellular automaton. LNCS 8751, pp. 125–135 (2014)
4. Alonso-Sanz, R.: On a three-parameter quantum battle of the sexes cellular automaton. Quantum Inf. Process. **12**(5), 1835–1850 (2013)
5. Alonso-Sanz, R.: A quantum battle of the sexes cellular automaton. Proc. R. Soc. A **468**, 3370–3383 (2012)
6. Alonso-Sanz, R.: Dynamical Systems with Memory. World Scientific Pub, Singapore (2011)
7. Benjamin, S.C., Hayden, P.M.: Comment on "Quantum games and quantum strategies". Phys. Rev. Lett. **87**(6), 069801 (2001)
8. Bleiler, S.: A formalism for quantum games and an application. http://arxiv.org/abs/0808.1389 (2008)
9. Branderburger, A.: The relationship between quantum and classical correlation games. Games Econ. Behav. **89**, 157–183 (2010)
10. Cheon, T., Iqbal, A.: Bayesian Nash equilibria and bell inequalities. J. Phys. Soc. Jpn. **77**(2), 024801 (2008). doi:10.1143/JPSJ.77.024801
11. Du, J., Ju, C., Li, H.: Quantum entanglement helps in improving economic efficiency. J. Phys. A Maths. Gen. **38**, 1559–1565 (2005)
12. Du, J.F., Xu, X.D., Li, H., Zhou, X., Han, R., et al.: Entanglement playing a dominating role in quantum games. Phys. Lett. A **89**(1–2), 9–15 (2001)
13. Du, J.F., Li, H., Xu, X.D., Zhou, X., Han, R.: Phase-transition-like behaviour of quantum games. J. Phys. A Math. Gen. **36**(23), 6551–6562 (2003)
14. Eisert, J., Wilkens, M., Lewenstein, M.: Quantum games and quantum strategies. Phys. Rev. Lett. **83**(15), 3077–3080 (1999)
15. Flitney, A.P., Abbott, D.: Advantage of a quantum player over a classical one in 2×2 quantum games. Proc. R. Soc. Lond. A **459**(2038), 2463–2474 (2003)
16. Flitney. A.P., Abbott, D.: An Introduction to quantum game theory. Fluct. Noise Lett. 02, R175. http://arxiv.org/pdf/quant-ph/0208069 (2002)
17. Frackiewicz, P.: A new quantum scheme for normal-form games. Process. Quantum Inf. (2015). doi:10.1007/s11128-015-0979-z
18. Iqbal, A., Chappell, J.M., Li, Q., Pearce, C.E.M., Abbott, D.: A probabilistic approach to quantum Bayesian games of incomplete information. Quantum Inf. Process. **13**(12), 2783–2800 (2014)
19. Khan, F.S.: Dominant Strategies in Two Qubit Quantum Computations. http://arxiv.org/abs/1410.0940 (2014)
20. Khan, F.S., Phoenix, S.J.D.: Mini-maximizing two qubit quantum computations. Quantum Inf. Process. **12**(12), 3807–3819 (2013)
21. Khan, F.S., Phoenix, S.J.D.: Gaming the quantum. Quantum Inf. Comput. **13**(3–4), 231–244 (2013)
22. Landsburg, S.E.: Quantum game theory. To appear in the The Wiley Encyclopedia of Operations Research and Management Science. http://arxiv.org/pdf/1110.6237v1 (2011)
23. Landsburg, S.E.: Quantum game theory. Notices of the AMS. http://www.ams.org/notices/200404/fea-landsburg (2004)
24. Levine, D.K.: Quantum games have no news for economists. http://levine.sscnet.ucla.edu/papers/quantumnonews (2005)
25. Marinatto, L., Weber, T.: A quantum approach to static games of complete information. Phys. Lett. A **272**, 291–303 (2000)
26. Meyer, D.A.: Quantum strategies. Phys. Rev. Lett. **82**, 1052–1055 (1999)
27. Miszczak, J.A., Pawela, L., Sladkowski, J.: General model for an entanglement-enhanced composed quantum game on a two-dimensional lattice. Fluct. Noise Lett. **13**(2) 1450012 (2014) http://arxiv.org/abs/1306.4506
28. Nawaz, A., Toor, A.H.: Dilemma and quantum battle of sexes. J. Phys. A Math. Gen. **37**(15), 4437 (2004)
29. Nawaz, A., Toor, A.H.: Generalized quantization scheme for two-person non-zero sum games. J. Phys. A Math. Gen. **37**(47), 11457 (2004)

30. Osborne, M.J., Rubinstein, A.: A Course in Game Theory. MIT Press, Cambridge (1994)
31. Owen, G.: Game Theory. Academic Press, New York (1995)
32. Pappa, A., Kumar, N., Lawson, T., Santha, M., Zhang, S., Diamanti, E., Kerenidis, I.: Nonlocality and conflicting interest games. Phys. Rev. Lett. **114**, 020401 (2015)
33. Phoenix, S.J.D., Khan, F.S.: The role of correlations in classical and quantum games. Fluct. Noise Lett. **12**(3), 1350011 (2013)
34. Piotrowski, E.W., Sladkowski, J.: An invitation to quantum game theory. Int. J. Theor. Phys. **42**(5), 1089–1099 (2003)
35. Situ, H.: A quantum approach to play asymmetric coordination games. Quantum Inf. Process. **13**(3), 591–599 (2013)
36. Situ, H.: Quantum Bayesian game with symmetric and asymmetric information. Quantum Inf. Process. **14**(6), 1827–1840 (2015)
37. Wiesner, K.: Quantum cellular automata. Encycl. Complex. Syst. Sci. 7154–7164. http://arxiv.org/0808.0679 (2009)